J MATER SCI **41** (2006) 2567–2571

Characterization of nanometer-sized Pt-dendrite structures fabricated on insulator Al_2O_3 substrate by electron-beam-induced deposition

GUOQIANG XIE*†, MINGHUI SONG, KAZUTAKA MITSUISHI, KAZUO FURUYA
High Voltage Electron Microscopy Station, National Institute for Materials Science, 3–13 Sakura, Tsukuba, 305-0003, Japan
E-mail: xiegq@imr.tohoku.ac.jp

Published online: 17 April 2006

Nanometer-sized Pt-dendrite structures were fabricated on an insulator Al_2O_3 substrate using an electron-beam-induced deposition (EBID) process in a transmission electron microscope (TEM). The as-fabricated structures were characterized using conventional and high-resolution transmission electron microscopies (CTEM and HRTEM) and X-ray energy dispersive spectroscopy (EDS). The as-fabricated nanodendrites consisted of many nano-grains and amorphous state structures. The nanometer-sized grains were determined to be Pt crystals with face-centered cubic (fcc) structure. The formation of the nanodendrite structures are discussed to relate to a mechanism involving charge-up produced on surface of the substrate, movement of charges to and accumulation at the convex surface of the substrate and the tips of the deposits. © *2006 Springer Science + Business Media, Inc.*

1. Introduction

Electron-beam-induced deposition (EBID) is one of the most promising processes for direct nanofabrication. It offers the ability to produce small-sized structures with high-resolution and high-position accuracy [1–3]. In this approach, an electron beam in a high-vacuum chamber is focused on a substrate surface on which precursor molecules (e.g., an organometallic compound or hydrocarbon), containing the element to be deposited are adsorbed. As a result of complex beam-induced surface reactions, the precursor molecules absorbed in or close to the irradiated area, are dissociated into nonvolatile and volatile parts by energetic electrons. The nonvolatile materials are deposited on the surface of the substrate to form a deposit, while the volatile components are pumped away by the vacuum system. Due to the control of the electron beam, fabrication of position-controlled nanostructures can be realized. Using the technique, a variety of nanometer-sized structures, such as nanodots, nanowires, nanotubes, nanopatterns, two- or three-dimensional nanoobjects, and so on, have been fabricated [1–14]. In these fabrications, conductive substrates are commonly considered to be suitable as they can easily reach a stable fabrication condition [11]. As a result, compact structures are usually fabricated with this process.

On the other hand, the nanofabrication with this technique using nonconductive substrates is also very important for the technique to be applied in technology. Recently, we fabricated nanometer-sized W-dendritic form structures on an Al_2O_3 insulator substrate with appropriate irradiation conditions by EBID process in a 200 kV transmission electron microscope (TEM) [15, 16]. We have investigated the effect of electron-beam accelerating voltage on *W*-nanodendrite structures. It was indicated that high-energy electron irradiation enhanced diffusion of W atoms in the nanodendrites, and hence promoted crystallization of *W* grains. More crystallized *W*-nanodendrite structures were achieved by EBID process using higher energy electron beams [17]. However, knowledge of the growth of the nanometer-sized structures with EBID process on insulator substrate is still very limited.

In the present study, nanometer-sized Pt-dendrite structures were fabricated on an insulator Al_2O_3

*Author to whom all correspondence should be addressed.
†*Present Address*: Institute for Materials Research, Tohoku University, Sendai 980-8577, Japan.
0022-2461 © *2006 Springer Science + Business Media, Inc.*
DOI: 10.1007/s10853-006-7769-z

substrate using an EBID process in a 200 kV TEM. The as-fabricated structures were characterized in detail using conventional and high-resolution transmission electron microscopies (CTEM and HRTEM) and X-ray energy dispersive spectroscopy (EDS).

2. Experimental methods

EBID was carried out using a TEM (JEOL, JEM-2010F) operated at an accelerating voltage of 200 kV. The field emission gun of the TEM makes the intensity of the electron beam controllable in a wide range. The base pressure in column was lower than 2×10^{-5} Pa. A cold trap filled with liquid nitrogen near the specimen holder was used to eliminate contamination by the residual gases in the column of the TEM. A gas introduction system including a nozzle and a reservoir of precursor source was installed on this microscope. The nozzle was located within 2 mm of the specimen. The inner diameter of the nozzle was smaller than 100 μm. (Methylcyclopentadienyl)trimethylplatinum powder, $Me_3MeCpPt$, was used as a precursor. The vapor pressure is approximately 10 Pa at room temperature. The flux of the gas near the specimen surface was estimated to be 1×10^{-4} PaL/s assuming molecular flow condition. At this flux, the measured value of the background pressure of the chamber did not change detectably.

Crystalline Al_2O_3 thin-film specimens suitable for TEM observation were used as substrates. The specimens were prepared from commercially obtained wafers by means of dimpling and argon ion milling. The current density of the electron beam for irradiating the specimens, which was estimated by measuring the total intensity and the size of electron beam at a working condition, was in the range from 0.23 to 2.1 A cm^{-2}. The size of the electron beam during irradiation was about 300 to 3000 nm. The fabricated structures were observed and analyzed *in situ* or after the fabrication with a JEM-2010F TEM operated at 200 kV and an EDS system attached to the TEM. A camera-video recorder system mounted under the camera chamber of JEM-2010F TEM was used to record the growth process. All the experiments were carried out at room temperature.

3. Results and discussion

3.1. Pt-nanodendrite structures

With the EBID process, Pt depositions were carried out on an insulator Al_2O_3 substrate in the TEM. Pt-nanodendrite-like structures were observed to grow in the area of the electron-beam irradiation. Fig. 1 shows TEM micrographs of nanodendrite-like structures grown on an Al_2O_3 substrate. The electron beam is defocused to a size of about 600 nm, corresponding to a current density of 0.52 A cm^{-2}. The irradiated time is 1 min. The irradiating fluence of the electron beam is 2.0×10^{20} e cm^{-2}. The edge of the electron beam is indicated by arrows in Fig. 1a. The contrast inside the irradiated area is obviously dark. The size of dendrite structures is much smaller than the diameter of the electron beam. The dendrites show a tendency to grow at the edge of the substrate. The dendrites have branches at the tip, as observed in Fig. 1b. The diameter of the nanodendrites becomes thicker near the substrate, which implies that the deposition takes place at both the tip and the trunk part. The typical thickness of the tips is less than 3 nm, as observed in Fig. 1b.

It has been reported previously that carbon dendrite-like structure can be formed from hydrocarbon molecules in the vacuum system on insulator substrates under electron-beam irradiation in the electron microscope at relatively poor vacuum conditions [18–20], as well as nanometer-sized *W*-dendrite structures were fabricated on insulator

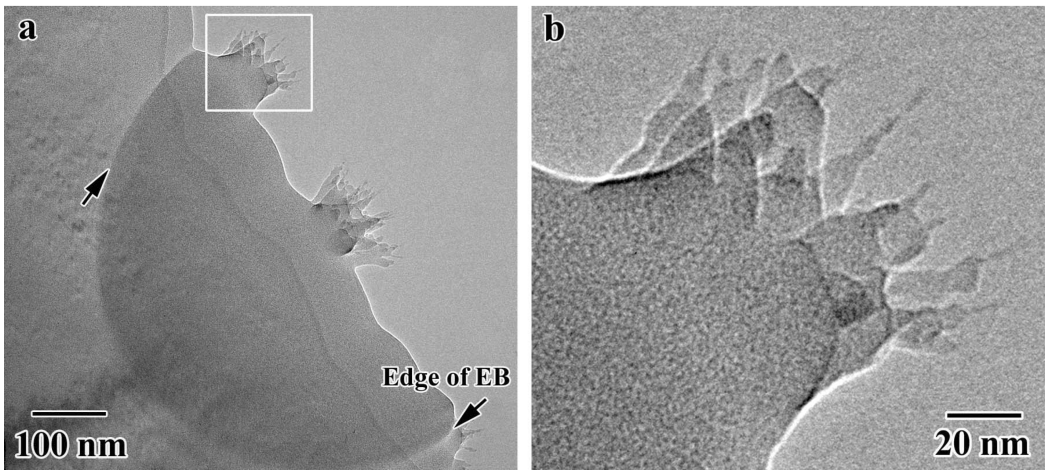

Figure 1 (a) TEM micrographs of Pt-nanodendrite structures grown on the surface of an Al_2O_3 substrate with an electron-beam-induced deposition (EBID) process 1 min after the start of the electron beam irradiation to a fluence of 2.0×10^{20} e cm^{-2}. (b) Enlargement of the square area in (a), showing the nanodendrites in more detail.

substrates with appropriate irradiation conditions with EBID process [15–17]. Charge-up effects have been generally considered to be a reason for the growth of the dendrite-like structures, since the charge-up may take place on the surface of an insulator substrate due to emission of secondary electrons under electron-beam irradiation.

It is well known that EBID is caused by the dissociation of molecules adsorbed to a surface by energetic electron beam. The molecule of a precursor is first adsorbed on surface of a substrate and then decomposed into volatile and nonvolatile parts by further irradiation of the energetic beam. The volatile component is pumped away by the vacuum system, while the nonvolatile fraction accumulates to form a deposit. The dissociation mechanism is complex and as yet not fully understood because of the huge number of excitation channels available even for small molecules. The details involving the decomposition have been argued to relate to secondary electrons on the surface of a specimen produced by the incident electron beam and backscattered electrons in an EBID process [3, 11]. On the surface of an electrically grounded conductive substrate, the molecules absorbed may move or not move, but distribute randomly and be decomposed on the surface. Therefore a compact deposit is usually formed [6–13].

On the other hand, in a case when the deposition is conducted on an insulator substrate, charge-up may take place on the surface. When specimens are exposed to electron bombardments, the molecules absorbed to a surface of a substrate or near the surface in the irradiated area may be polarized by irradiation of the incident electron beam. The irradiated area on the insulator substrate is easily charged and forms a local electric field. Due to the Coulomb interaction in an electric field on the surface, these polarized molecules are attracted to the irradiated area. They are decomposed and form a deposit. The distribution of charges due to charge-up on the surface may not be even on a nanometer scale. This unevenness may be due to the nanoscale roughness or atomic steps on the surface. Charges may accumulate on the surface of the substrate or the deposit, and tend to move to places with convex surface, such as a convex edge, especially sharp tips. The denser charges are accumulated in these places. The built-up electric field may be stronger than in the surrounding regions. Therefore, movable precursor molecules from both the surface and outside of the substrate may be attracted to these places. After a deposit is formed, charges may move and accumulate at its tip, hence the deposit will grow longer under the continued electron beam irradiation. Since the built-up electric field near a tip may not influence the flying of a molecule very much, the deposit grows at both its tip and its trunk part due to molecules coming to tips and trunk at the same time. The deposit will grow thicker at its trunk part with increasing the time and thus develop a dendrite-like morphology. Therefore, the movement and accumulation of charges play a key role in the formation of the dendrite-like structure.

3.2. Characterization of as-fabricated nanodendrites

Characterization of the as-fabricated nanodendrite structures was carried out with CTEM, HRTEM and EDS. It reveals that nanometer-sized Pt grains with fcc structure are contained in the deposits. Fig. 2 shows TEM micrographs of the as-grown dendrite structures fabricated with EBID process to a fluence of 2.6×10^{21} e cm^{-2}. Figs2 a and b give a bright-field (BF) micrograph and the corresponding selected-area diffraction (SAD) pattern, respectively. Fig. 2c shows a dark-field (DF) TEM image corresponding to Fig. 2a using part of the ring corresponding to $d_1 = 0.227$ nm in Fig. 2b. A lot of bright contrast dots are observed, and considered to be small Pt grains.

Fig. 3 is an HRTEM micrograph of a nanodendrite structure fabricated during an electron beam irradiating fluence of 2.6×10^{21} e cm^{-2}. It is seen that the as-fabricated nanodendrite structures consist of a mixture of nano-grains embedded in an amorphous matrix. The size of the nano-grains is about 3 nm. Lattice fringes are observed clearly in the nano-grains. The largest and also the most frequently observed lattice spacing measured from this figure as well as from other HRTEM micrographs is 0.22 nm. It is close to the lattice spacing, 0.227 nm, of $\{111\}$ of bulk metal fcc Pt crystals with a deviation smaller than 5%. Moreover, lattice fringes with spacing $d = 0.22$ nm have inter-fringe angle of 70.5 degrees (such as grain A), as indicated in Fig. 3. They agree with the zone axis of [110] of the fcc Pt structure. Furthermore, HRTEM micrographs taken from other regions or other dendrites present similar results. The diffraction pattern analyses in Fig. 2b where several diffuse rings are observed indicate the existence of very small crystals in the nanodendrite structures in accordance with the observation in the images. It is seen that these diffraction rings correspond to lattice spacing of about 0.227, 0.196, 0.138, 0.118, and 0.089 nm, respectively that are in good agreement with those of bulk fcc Pt of $\{111\}$, $\{200\}$, $\{220\}$, $\{311\}$, and $\{331\}$. It is noted that the as-fabricated nanodendrites consist of many nanometer-scale fcc Pt crystals.

Further characterization of the as-fabricated nanodendrite structures was performed with EDS analyses. It is confirmed that Pt, the targeted element, has been effectively deposited in the nanodendrite structures. Fig. 4 shows EDS spectra taken from an as-deposited nanodendrite corresponding to Fig. 3. Fig. 4a presents a spectrum taken from the area with nano-grain, and Fig. 4b gives that from the area with amorphous state structure. The size of

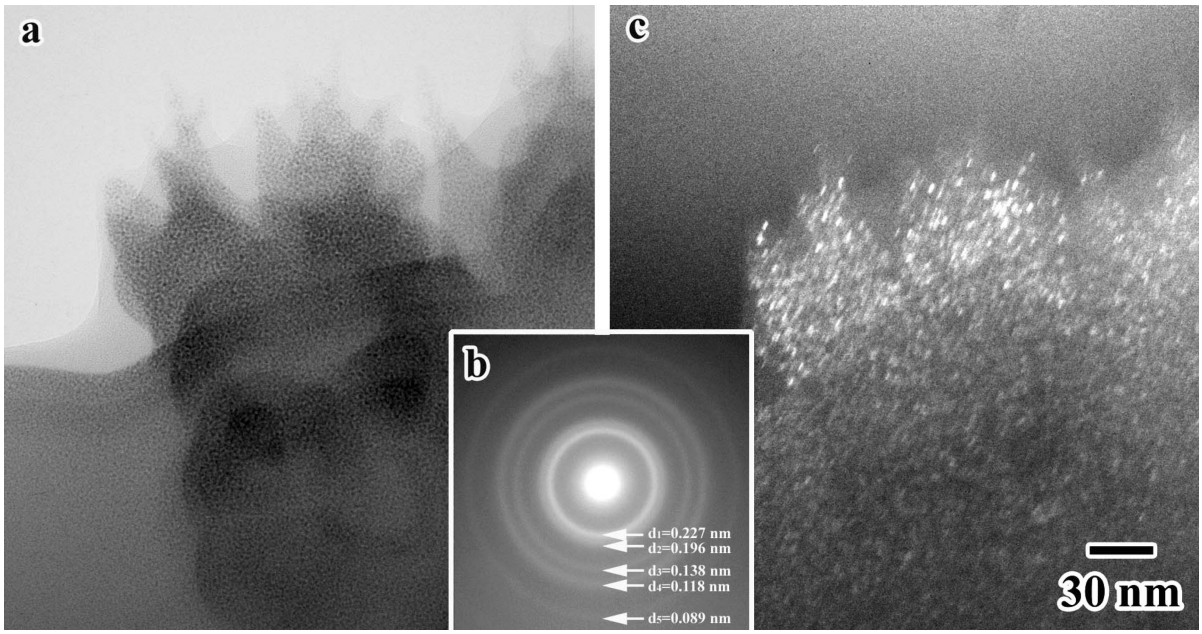

Figure 2 TEM micrographs of the as-fabricated dendrite structures irradiating to a fluence of 2.6×10^{21} e cm^{-2}. (a) a bright-field (BF) TEM image; (b) a selected-area diffraction (SAD) pattern; (c) a corresponding dark-field (DF) TEM image of (a) using part of the ring with $d_1 = 0.227$ nm in (b).

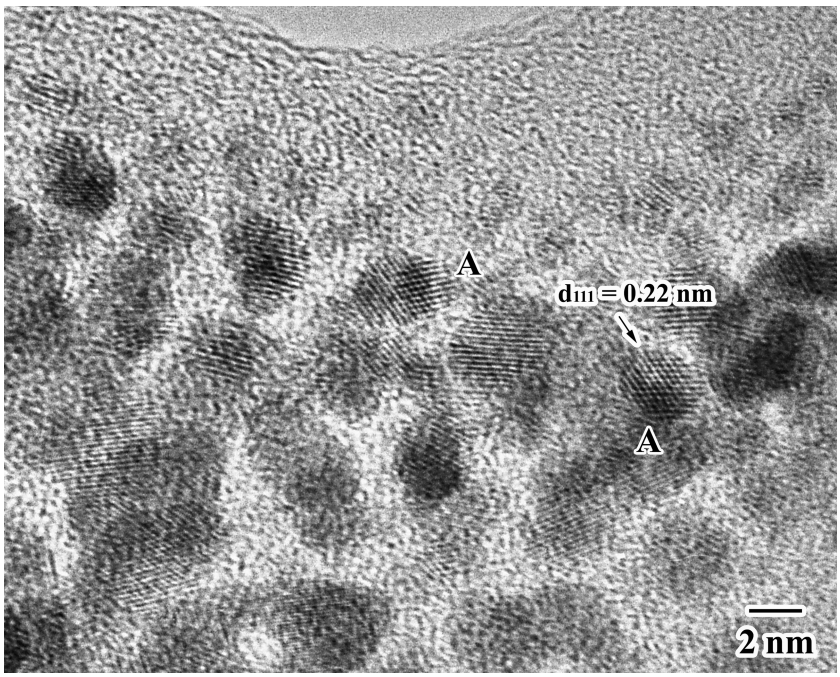

Figure 3 An HRTEM micrograph of a nanodendrite structure fabricated on an electron beam irradiating fluence of 2.6×10^{21} e cm^{-2}.

electron beam for the EDS analysis is about 3 nm. It is clear that the peaks of Pt dominate these spectra, as indicated in Fig. 4. No obvious difference of the composition between the area with nano-grains and the amorphous state is observed, except a little higher carbon content in amorphous state. Based on the EDS spectra, the relative contents of 67.4% Pt compared with 32.6% C for the area with nano-grains and 60.0% Pt with 40.0% C for that with amorphous state are obtained. The relative content of Pt is higher than the reported result of the Pt deposits fabricated at an electron beam energy (20 keV) in the EBID process, which is 14% [21]. Similar results were also obtained by analyses of other nanodendrites. Combined with TEM observations, diffraction pattern analyses, and EDS analyses, it is indicated that nanodendrite structures with a high Pt content are formed. The as-fabricated

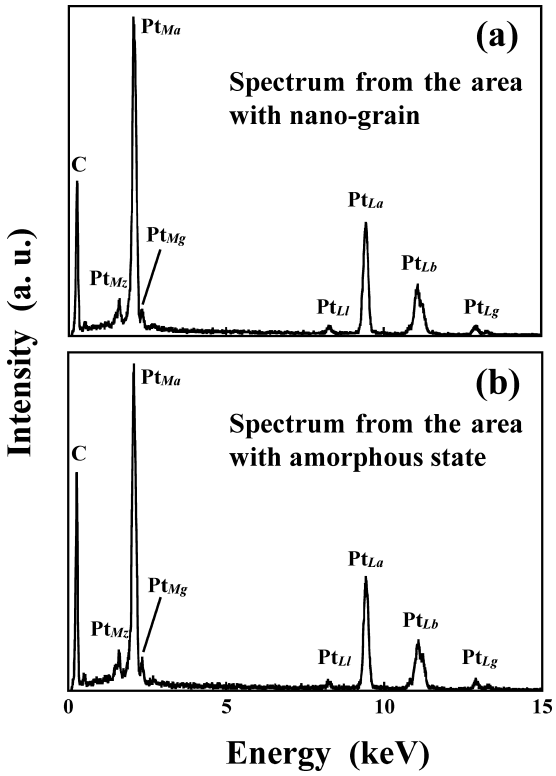

Figure 4 EDS spectra taken from an as-deposited nanodendrite corresponding to Fig. 3. (a) a spectrum taken from the area with nano-grain; (b) a spectrum taken from the area with amorphous state structure. The size of electron beam for the EDS analysis is about 3 nm.

nanodendrites consist of many nanometer-sized grains embedded in an amorphous state structures. The nanometer-sized grains are determined to be Pt crystal with fcc structure.

4. Conclusions

Nanometer-sized Pt-dendrite structures were fabricated on an insulator Al_2O_3 substrate using an EBID process in a 200 kV TEM. The as-fabricated structures were characterized using CTEM, HRTEM, and EDS. Nanodendrite structures with a high Pt content are formed. The as-fabricated nanodendrites consist of many nano-grains and amorphous state structures. The nanometer-sized grains are determined to be Pt crystals with fcc structure. The formation of the nanodendrite structures are anticipated to contribute to a mechanism involving charge-up produced on the surface of the substrate, movement of charges to and accumulation at the convex surface of the substrate and the tips of the deposits.

References

1. K. MITSUISHI, M. SHIMOJO, M. HAN and K. FURUYA, *Appl. Phys. Lett.* **83** (2003) 2064.
2. V. V. ARISTOV, A. YU KASUMOV, N. A. KISLOV, O. V. KONONENKO, V. N. MATVEEV, V. A. TULIN, I. I. KHODOS, YU A. GORBATOV and V. I. NIKOLAICHIK, *Nanotechnology* **6** (1995) 35.
3. H. W. P. KOOPS, R. WEIEL, D. P. KERN and T. H. BAUM, *J. Vac. Sci. Technol. B* **6B** (1988) 477.
4. G. Q. XIE, M. SONG, K. MITSUISHI and K. FURUYA, *Appl. Phys. A* **79** (2004) 1843.
5. *Idem., J. Vac. Sci. Technol. B* **22** (2004) 2589.
6. L. X. DONG, F. ARAI and T. FUKUDA, *Appl. Phys. Lett.* **81** (2002) 1919.
7. S. MATSUI, T. KAITO, J. FUJITA, M. KOMURA, K. KANDA and Y. HARUYAMA, *J. Vac. Sci. Technol. B* **18** (2000) 3181.
8. I. UTKE, P. HOFFMANN, B. DWIR, K. LEIFER, E. KAPON and P. DOPPELT, *Ibid B* **18** (2000) 3168.
9. H. HIROSHIMA, N. SUZUKI, N. OGAWA and M. KOMURO, *Jpn. J. Appl. Phys. Part 1* **38** (1999) 7135.
10. H. BRUCKL, J. KRETZ, H. W. KOOPS and G. REISS, *J. Vac. Sci. Technol. B* **17** (1999) 1350.
11. P. C. HOYLE, J. R. A. CLEAVER and H. AHMED, *Ibid B* **14** (1996) 662.
12. H. W. P. KOOPS, J. KRETZ, M. RUDOLPH, M. WEBER, G. DAHM and K. L. LEE, *Jpn. J. Appl. Phys. Part 1* **33** (1994) 7099.
13. K. T. KOHLMANN-VON PLATEN, J. CHLEBEK, M. WEISS, K. REIMER, H. OERTEL and W. H. BRUNGER, *J. Vac. Sci. Technol. B* **11** (1993) 2219.
14. G. Q. XIE, M. SONG, K. MITSUISHI and K. FURUYA, *Appl. Surf. Sci.* **241** (2005) 91.
15. M. SONG, K. MITSUISHI, M. TANAKA, M. TAKEGUCHI, M. SHIMOJO and K. FURUYA, *Appl. Phys. A* **80** (2005) 1431.
16. M. SONG, K. MITSUISHI, M. TAKEGUCHI and K. FURUYA, *Appl. Surf. Sci.* **241** (2005) 107.
17. G. Q. XIE, M. SONG, K. MITSUISHI and K. FURUYA, *J. Nanosci. Nanotechno.* **5** (2005) 615.
18. H. Z. WANG, X. H. LIU, X. J. YANG and X. WANG, *Mat. Sci. Eng. A* **311** (2001) 180.
19. J. Z. ZHANG, X. Y. YE, X. J. YANG and D. LIU, *Phys. Rev. E* **55** (1997) 5796.
20. F. BANHART, *Phys. Rev. E* **52** (1995) 5156.
21. H. W. P. KOOPS, A. KAYA and M. WEBER, *J. Vac. Sci. Technol. B* **13B** (1995) 2400.